Electronic Supplementary Information

Experimental section

Materials: Carbon cloth (CC) was obtained from Hongshan District, Wuhan Instrument Surgical Instruments business and pretreated in HNO_3 for further application. $Fe(NO_3)_3 \cdot 9H_2O$ was supported by Tianjin Fuyu Chemical Reagent Co. Ltd. $Co(NO_3)_2 \cdot 6H_2O$, NH_4F, $K_2B_4O_7 \cdot 4H_2O$ and urea were provided by Chengdu Kelong Chemical Reagent Factory. Nafion (5 wt%) and $RuCl_3 \cdot 3H_2O$ were bought from Sigma-Aldrich Chemical Reagent Co., Ltd. Water used in all experiments was obtained from a Millipore purified system. All the reagents were used as received without further purification.

Preparation of $CoFe_2O_4$/CC, Co_3O_4/CC and Fe_3O_4/CC: $CoFe_2O_4$/CC was prepared as follows. $Co(NO_3)_2 \cdot 6H_2O$ (1 mmol), $Fe(NO_3)_3 \cdot 9H_2O$ (2 mmol), urea (5 mmol) and NH_4F (2 mmol) were dissolved in 30 ml distilled water and stirred for 15 min. The resulting solution was transferred to a 50 mL Teflon-lined autoclave with a piece of CC (2 cm × 4 cm), which had been cleaned by sonication in water and ethanol for 10 min. The autoclave was sealed and kept at 120 °C for 10 h in an electric oven. After being cooled to room temperature, the CC was cleaned with water and ethanol for several times and dried at 60 °C. Subsequently, the sample was calcined at 450 °C in Ar atmosphere for 2 h to obtain $CoFe_2O_4$/CC. Fe_3O_4/CC and Co_3O_4/CC were made without the addition of $Fe(NO_3)_3 \cdot 6H_2O$ or $Co(NO_3)_2 \cdot 6H_2O$, respectively.

Synthesis of $CoFe_2O_4$@Co-Fe-Bi/CC, Co_3O_4 and Fe_3O_4 nanoarray-derived catalysts: To obtain $CoFe_2O_4$@Co-Fe-Bi/CC, $CoFe_2O_4$/CC was treated at 1 V (vs. Ag/AgCl) as the working electrode in 0.1 M K-Bi (pH 9.2) for 0.5 h. A platinum wire and an Ag/AgCl were used as the counter electrode and the reference electrode, respectively. Co_3O_4 and Fe_3O_4-derived nanoarray catalysts were prepared similarly from Fe_3O_4/CC and Co_3O_4/CC.

Synthesis of RuO_2: RuO_2 was synthesized according to previous report.[1] In a typical synthesis, 2.61 g of $RuCl_3 \cdot 3H_2O$ was dissolved into 100 ml distilled water and stirred for 10 min at 100 °C. Then 1.0 ml KOH (1.0 M) was added into the above solution

and stirred for 45 minutes. The precipitates were collected and washed with water for several times, further dried at 80 °C overnight and then annealed at 300 °C in air atmosphere for 3 h.

Characterizations: Powder X-ray diffraction (XRD) patterns were performed using a RigakuD/MAX 2550 diffractometer with Cu Kα radiation (λ=1.5418 Å). Scanning electron microscope (SEM) measurements were recorded on a XL30 ESEM FEG scanning electron microscope at an accelerating voltage of 20 kV. Transmission electron microscopy (TEM) images were observed on a HITACHI H-8100 electron microscopy (Hitachi, Tokyo, Japan) operated at 200 kV. X-ray photoelectron spectroscopy (XPS) was conducted on an ESCALABMK II x- ray photoelectron spectrometer using Mg as the exciting source.

Electrochemical measurements: Electrochemical measurements were performed with a CHI 660E electrochemical analyzer (CH Instruments, Inc., Shanghai) in a standard three-electrode system. $CoFe_2O_4$@Co-Fe-Bi/CC was used as the working electrode, a platinum wire as the counter electrode and a Ag/AgCl as the reference electrode in K-Bi. The experimental temperature was kept at 25 °C for all electrochemical measurements. All the potentials were calibrated to RHE other than especially stated, following the equation: E (RHE) = E (Ag/AgCl) + (0.197 + 0.059 pH) V.

TOF calculations: For direct comparison with other catalysts, TOF was calculated based on the surface concentration of active sites related to the Co and Fe species. According to the electrochemical cyclic voltammetry curves, the oxidation peak current of redox species presents linear change on scan rates (Fig. S6). The slope of the line can be calculated by the following equation:

$$\text{Slope} = n^2F^2A\Gamma_0 /4RT$$

Where n is the number of electrons transferred, which is denoted as 1 in order to achieve the upper limit in concentration of active sites; F is Faraday's constant (96485 C mol^{-1}); A is the surface area of the electrode (0.25 cm^{-2}); Γ_0 is the surface concentration of active sites (mol cm^{-2}), and R and T are the ideal gas constant (8.314 J mol^{-1} k^{-1}) and the absolute temperature (298 K), respectively.

TOF values can be finally calculated from the formula:

$$TOF = JA/4Fm$$

Where J is the current density under certain overpotential, A is the area of the electrode (0.25 cm^{-2}), 4 indicates the mole of electrons consumed for evolving one mole of O_2 from water, F is Faraday's constant (96485 C mol^{-1}) and m is the number of moles of active sites.

FE determination: FE was calculated by comparing the amount of the oxygen generated at anode with theoretically calculated gas. The experimentally evolved oxygen was confirmed by gas chromatography (GC) analysis and quantified by monitoring the pressure change via a calibrated pressure sensor in the anode compartment of a H-type electrolytic cell. The quantity of theoretically generated oxygen was calculated by assuming that all charges through the anode were $4e^-$ oxidation to produce oxygen.

Computational Methods: All density-functional theory (DFT) calculations in this study were performed using the Vienna *ab initio* simulation package (VASP).[2-4] We used the PBE functional for the exchange-correlation energy[5] and projector augmented wave (PAW) potentials.[6,7] The kinetic energy cutoff in the calculation was set to 450 eV. The ionic relaxation was performed until the force on each atom is less than 0.03 eV/Å and convergence criteria of total energy were set to 10^{-4} eV. The 3×3×1 k-points meshes were sampled based on the Monkhorst-Pack method.[7] The Hubbard U parameter (GGA+U) with U=4 eV was used to calculate the electron correlation within the Fe and Co ions. The Bader charge analysis was used to calculate the charge transfer in CoBi, FeBi and CoFeBi.[9] The simulations performed were based on a periodical model structure with 24 cobalt (or iron), 16 boron and 48 oxygen atoms. In fact, we found that the essential results are relatively insensitive to the selected model structures. To minimize the undesired interactions between images, a vacuum of at least 15 Å was considered along the z axis.

Previous studies have shown that the OER activity is strongly correlated with the free energy of O*, OH* and OOH* binding to the electrocatalysts surface. The four step OER mechanism is proposed as:

$$2H_2O + * \rightarrow OH^* + H_2O + e^- + H^+ \quad (1)$$

$$OH^* + H_2O \rightarrow O^* + H_2O + e^- + H^+ \quad (2)$$

$$O^* + H_2O \rightarrow OOH^* + e^- + H^+ \quad (3)$$

$$OOH^* \rightarrow O_2 + e^- + H^+ \quad (4)$$

The free energy (ΔG_i) for O*, OH* and OOH* adsorption on Co-Bi and $Co_{0.33}$-$Fe_{0.67}$-Bi surfaces was calculated as follows:

$$\Delta G_i = \Delta E_i + \Delta E_{ZPE} - T\Delta S \quad (5)$$

where ΔE_i is the reaction energy for each elementary step, ΔE_{ZPE} is the zero-point energy change and ΔS is the entropy change. The theoretical overpotential can be defined as:

$$\boldsymbol{\eta} = \max[\Delta G_1, \Delta G_2, \Delta G_3, \Delta G_4]/e - 1.23[V] \quad (6)$$

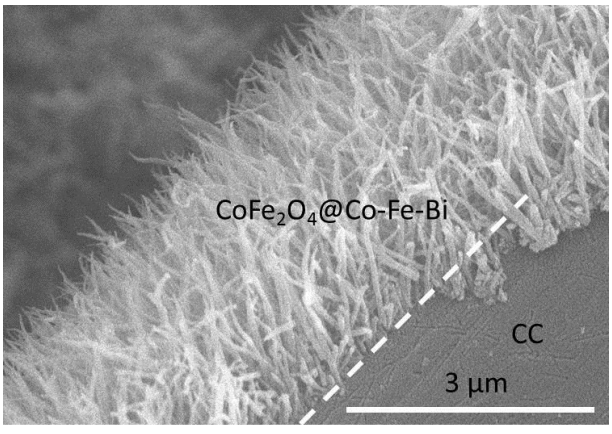

Fig. S1. The cross-sectional SEM image of $CoFe_2O_4$@Co-Fe-Bi/CC

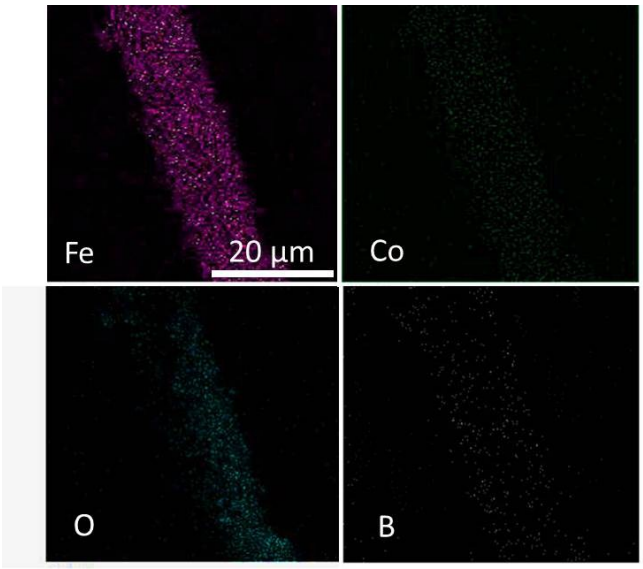

Fig. S2. EDX elemental mapping images of Fe, Co, O and B for $CoFe_2O_4$@Co-Fe-Bi/CC.

.

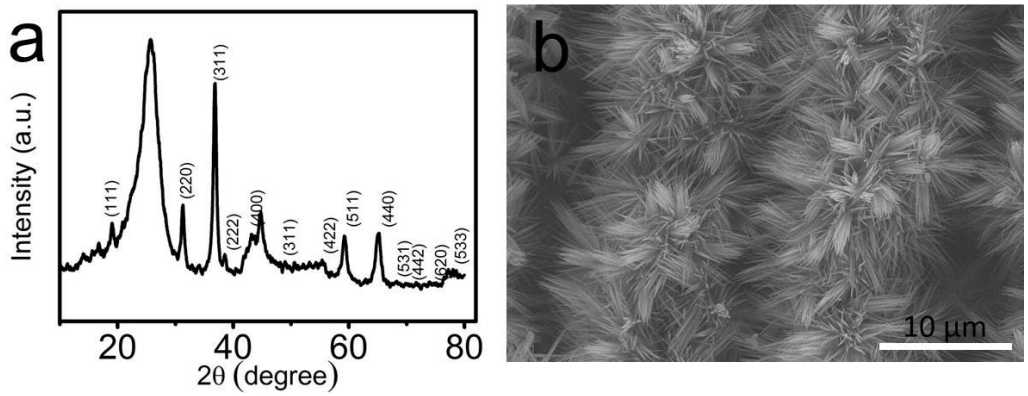

Fig. S3. (a) XRD patterns of Co_3O_4/CC. (b) SEM image for Co_3O_4/CC.

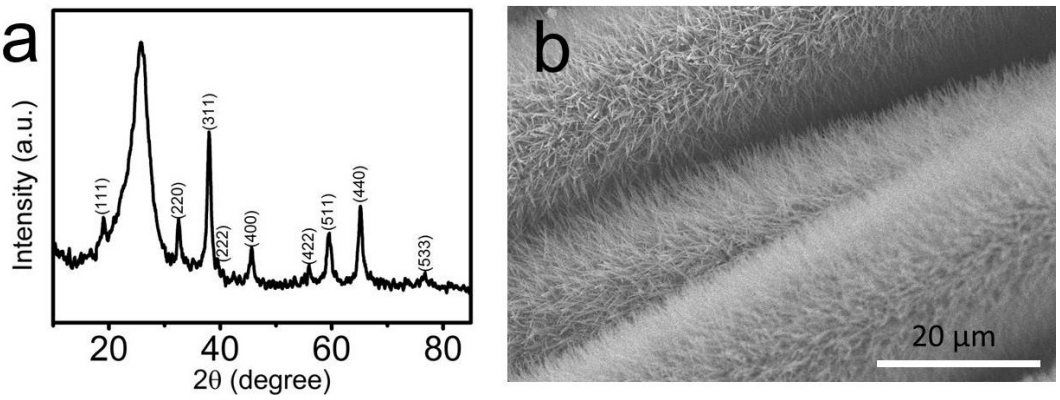

Fig. S4. (a) XRD patterns of Fe_3O_4/CC. (b) SEM image for Fe_3O_4/CC.

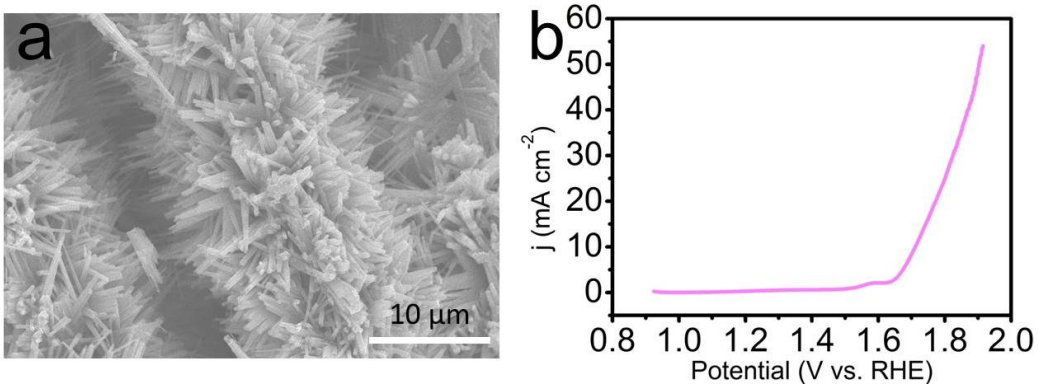

Fig. S5. (a) SEM image of Co_3O_4-derived nanoarray catalyst. (b) LSV curve for such catalyst with a scan rate of 5 mV s^{-1} for OER in 0.1 M K-Bi.

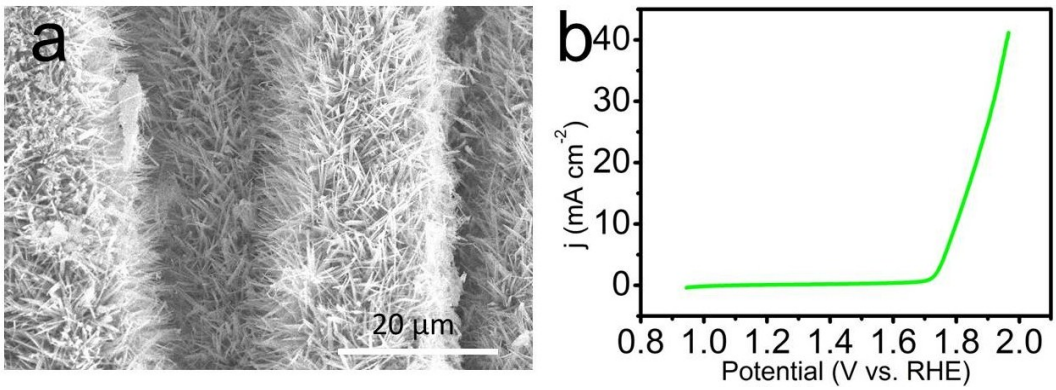

Fig. S6. (a) SEM image of Fe_3O_4-derived nanoarray catalyst. (b) LSV curve for such catalyst with a scan rate of 5 mV s^{-1} for OER in 0.1 M K-Bi.

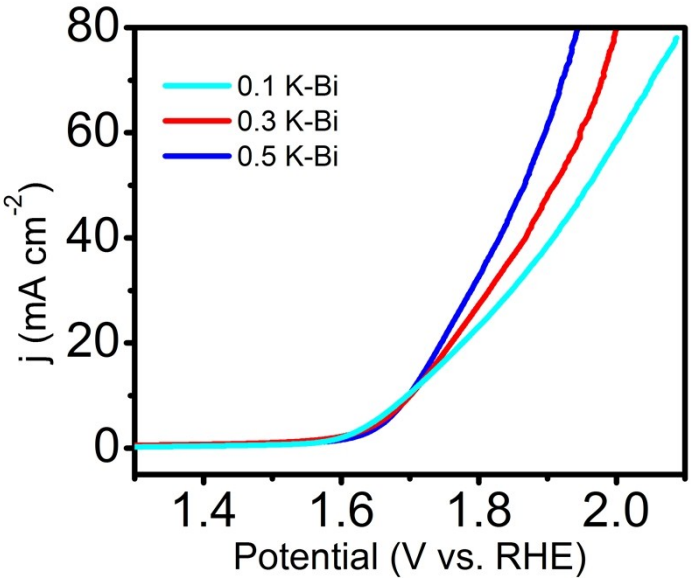

Fig. S7. LSV curves for $CoFe_2O_4$@Co-Fe-Bi/CC in 0.1, 0.3, and 0.5 M K-Bi for OER.

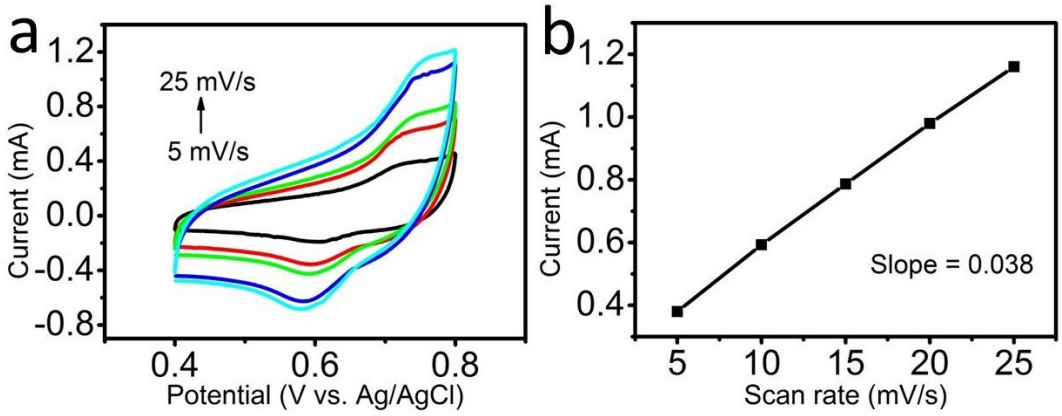

Fig. S8. (a) Cyclic voltammograms of $CoFe_2O_4$@Co-Fe-Bi/CC at different scan rates increasing from 5 to 25 mV s^{-1} with an increment of 5 mV s^{-1} in 0.1 M K-Bi. (b) Oxidation peak current versus scan rate plot for $CoFe_2O_4$@Co-Fe-Bi/CC.

Table S1. Comparison of OER performance for $CoFe_2O_4$@Co-Fe-Bi /CC with other non-noble-metal electrocatalysts in benign media.

Catalyst	j (mA cm^{-2})	η (mV)	Electrolyte	Ref.
$CoFe_2O_4$@Co-Fe-Bi /CC	1	330	0.1 M K-Bi	This work
	5	410	0.1 M K-Bi	
	10	460	0.1 M K-Bi	
Ni-4Gly	1	480	0.25 M PBS	10
Co_3O_4 nanorod	1	385	0.1 M PBS	11
MnO/FTO	5	530	0.3 M Na-Pi	12
Co-Ni LDH/FTO	1	490	0.1 M K-Pi	13
Fe-Bi film	1	470	0.5 M BBS	14
Fe-Ci/FTO	10	560	0.2 M Ci	15
Cu_2O/FTO	0.1	430	0.1 M K-Bi	16
Ni-Bi film/FTO	1	540	0.5 M K-Bi	17
Ni-Bi film/ITO	1	425	0.1 M Bi	18
Ni-Bi/CC	10	470	0.1 M K-Bi	19
Co-Bi/Ti	10	469	0.1 M K-Bi	20
Fe-P_i-B_i/CC	10	434	0.1 M K-B_i	21
Co-Pi/Ti	10	450	0.1 M PBS	22
CCH@Co-Pi NA/Ti	10	460	0.1 M PBS	23

References

1 J. C. Cruz, V. Baglio, S. Siracusano, V. Antonucci, A. S. Aricò, R. Ornelas, L.

Ortiz-Frade, G. Osorio-Monreal, S. M. Durón-Torres and L. G. Arriaga, *Int. J. Electrochem. Sci.*, 2011, **7**, 6607-6619.

2 G. Kresse and J. Furthmüller, *J. Comp. Mater. Sci.*, 1996, **6**, 15-50.

3 G. Kresse and J. Furthmüller, *J. Phys. Rev. B*, 1996, **54**, 11169-11186.

4 G. Kresse and J. Hafner, *J. Phys. Rev. B*, 1994, **49**, 14251-14269.

5 J. P. Perdew, K. Burke and M. Ernzerhof, *Phys. Rev. Lett.*, 1996, **77**, 3865-3868.

6 G. Kresse and D. Joubert, *Phys. Rev. B*, 1999, **59**, 1758-1775.

7 P. E. Blochl, *Phys. Rev. B,* 1994, **50**, 17953-17979.

8 H. J. Monkhorst, *Phys. Rev. B*, 1976, **13**, 5188-5192.

9 W. J. Orville-Thomas, *J. Mol. Struct.*, 1996, **360**, 175.

10 D. Wang, G. Ghirlanda and J. P. Allen, *J. Am. Chem. Soc.*, 2014, **136**, 10198-10201.

11 R. M. Ramsundar, J. Debgupta, V. K. Pillai and P. A. Joy, *Electrocatal.*, 2015, **6**, 331-340.

12 K. Jin, A. Chu, J. Park, D. Jeong, S. E. Jerng, U. Sim, H. Y. Jeong, W. Chan, Y. S. Park and K. Yang, *Sci. Rep.*, 2014, **5**, 10279.

13 Y. Zhang, B. Cui, C. Zhao, H. Lin and J. Li, *Phys. Chem. Chem. Phys.*, 2013, **15**, 7363-7369.

14 D. R. Chowdhury, L. Spiccia, S. S. Amritphale, A. Paul and A. Singh, *J. Mater. Chem. A*, 2016, **4**, 3655-3660.

15 F. Li, L. Bai, H. Li, Y. Wang, F. Yu and L. Sun, *Chem. Commun.*, 2016, **52**, 5753-5756.

16 X. Liu, Z. Sun, S. Cui and P. Du, *Electrochim. Acta*, 2015, **187**, 381-388.

17 I. Roger and M. D. Symes, *J. Am. Chem. Soc.*, 2015, **137**, 13980-13988.

18 M. Dincă, Y. Surendranath and D. G. Nocera, *Proc. Natl. Acad. Sci. U. S. A.*, 2010, **107**, 10337-10341.

19 X. Ji, L. Cui, D. Liu, S. Hao, J. Liu, F. Qu, Y. Ma, G. Du, A. M. Asiri and X. Sun, *Chem. Commun.,* 2017, **53**, 3070-3073.

20 L. Yang, D. Liu, S. Hao, R. Kong, A. M. Asiri, C. Zhang and X. Sun, *J. Mater. Chem. A*, 2017, **5**, 7305-7308.

21 W. Wang, D. Liu, S. Hao, F. Qu, Y. Ma, G. Du, A. M. Asiri, Y. Yao and X. Sun, *Inorg. Chem.*, 2017, **56**, 3131-3135.

22 L. Xie, R. Zhang, L. Cui, D. Liu, S. Hao, Y. Ma, G. Du, A. M. Asiri and X. Sun, *Angew. Chem., Int. Ed.*, 2017, **56**, 1064-1068.

23 L. Cui, D. Liu, S. Hao, F. Qu, G. Du, J. Liu, A. M. Asiri and X. Sun, *Nanoscale*, 2017, **9**, 3752-3756.